

Fusion hindrance for a positive Q -value system

C. L. Jiang,¹ B. B. Back,¹ H. Esbensen,¹ J. P. Greene,¹ R. V. F. Janssens,¹ D. J. Henderson,¹ H. Y. Lee,¹ C. J. Lister,¹
M. Notani,¹ R. C. Pardo,¹ N. Patel,¹ K. E. Rehm,¹ D. Seweryniak,¹ B. Shumard,¹ X. Wang,¹ S. Zhu,¹ S. Mişicu,²
P. Collon,³ and X. D. Tang³

¹*Physics Division, Argonne National Laboratory, Argonne, Illinois 60439, USA*

²*National Institute for Nuclear Physics, Bucharest, P.O. Box MG6, Romania*

³*University of Notre Dame, Notre Dame, Indiana 46556, USA*

(Received 7 May 2008; published 8 July 2008)

An excitation function for the fusion reaction $^{28}\text{Si} + ^{30}\text{Si}$ ($Q = 14.3$ MeV) has been measured down to $40 \mu\text{b}$. Deviations from the behavior predicted by the optical model and standard coupled-channels calculations have been observed in this system. The fusion cross sections can be reproduced by a shallow potential model well, which was originally developed to explain the hindrance of heavy-ion fusion for systems with negative Q -values.

DOI: [10.1103/PhysRevC.78.017601](https://doi.org/10.1103/PhysRevC.78.017601)

PACS number(s): 25.70.Jj, 25.60.Pj, 26.50.+x, 26.30.-k

Hindrance in heavy-ion fusion at extreme sub-barrier energies was discovered several years ago [1]. The phenomenon was first observed in medium-mass systems, but later measurements and analyses [2–7] showed that this might represent a general behavior of heavy-ion fusion at extreme sub-barrier energies. A systematic has been established for a wide mass region, showing that the hindrance is closely related to the entrance channel properties [5–7]. This hindrance could also affect fusion reactions that are of importance in nuclear astrophysics, such as $^{12}\text{C} + ^{12}\text{C}$ [6,8]. There is, however, an important difference between the systems studied earlier and the astrophysically important fusion reactions coming from the reaction Q -values: these are positive for lighter nuclei and negative for the medium-mass systems studied previously. In this experiment we have, therefore, measured a fusion excitation function in the system $^{28}\text{Si} + ^{30}\text{Si}$, which has a Q -value of 14.3 MeV, very close to that of the $^{12}\text{C} + ^{12}\text{C}$ reaction ($Q = 13.9$ MeV).

The fusion of $^{28}\text{Si} + ^{30}\text{Si}$ was studied previously by Gary and Volent [9] down to cross sections of about 17 mb, i.e., to an energy region much higher than the energy where fusion hindrance might occur. The new experiment was performed at the superconducting linear accelerator ATLAS at Argonne National Laboratory. The ^{28}Si beams delivered were in the energy range of 48.5–71 MeV. The isotopic abundance of the ^{30}Si target was 96.02%, with the remainder coming from ^{29}Si (0.33%) and ^{28}Si (3.43%). Thin targets with thicknesses of about $20 \mu\text{g}/\text{cm}^2$ SiO_2 (evaporated on $40 \mu\text{g}/\text{cm}^2$ carbon foils) were used in order to minimize the target thickness corrections in the energy regime where a steep fall-off in the excitation function occurs. The contaminations from lighter Si isotopes did not interfere with the actual measurements since the associated Coulomb barriers are higher than the one for ^{30}Si . Two surface-barrier Si detectors, located at $\pm 45^\circ$ with respect to the beam direction, were used for beam particle normalization.

The experimental procedure was similar to that used in earlier measurements of the fusion-evaporation excitation functions for the systems $^{28}\text{Si} + ^{64}\text{Ni}$ ($Q = -1.78$ MeV) and $^{64}\text{Ni} + ^{100}\text{Mo}$ ($Q = -92.29$ MeV) [1]. The evaporation

residues were measured with the Fragment Mass Analyzer (FMA) [10], placed at 0° with respect to the beam direction. This instrument has been upgraded with the installation of a split-anode in the first electric dipole, resulting in a suppression of the background originating mostly from beam particles scattered off the first anode. The evaporation residues were detected and identified behind the FMA with detectors of the configuration PGAC₁-TIC₁-PGAC₂-TIC₂-PGAC₃-IC (see Ref. [11] for further details). Here, the symbol PGAC stands for an x - y position-sensitive, parallel-grid avalanche counter, TIC for a transmission ionization chamber, and IC for a large volume multi-anode ionization chamber. The first PGAC₁ counter was mounted at the focal-plane of the FMA, where the evaporation residues are dispersed according to their mass-to-charge ratio m/q . Full charge state distributions were measured for four energies, while four to five charge states were recorded for five intermediate points. At the four lowest energies, only one or two charge states were measured because only one charge state could be measured at the time for each FMA setting. These data proved sufficient to determine the charge state fractions of the detected evaporation residues with the required accuracy.

In order to determine the FMA transmission it is necessary to characterize the angular distribution of the evaporation residues. In the present experiment this was achieved by using the statistical model code PACE [12]. It was found that the total angular distribution changes very little over the range of beam energies measured, thus making the efficiency corrections quite simple.

The system measured here is much lighter than the ones we have measured in our previous fusion hindrance studies [1]. The large differences in velocity (time of flight) and energy deposited in the detectors between the beam particles (or reaction particles from the contaminants in the target) and the evaporation residues observed in the previous experiments allowed us to measure the excitation function down to the tens of nb region. In the $^{28}\text{Si} + ^{30}\text{Si}$ system the separation between the evaporation residues and others was still sufficient at the higher incident energies. At the lowest energy of 48.5 MeV (corresponding to a cross section of about $40 \mu\text{b}$) the

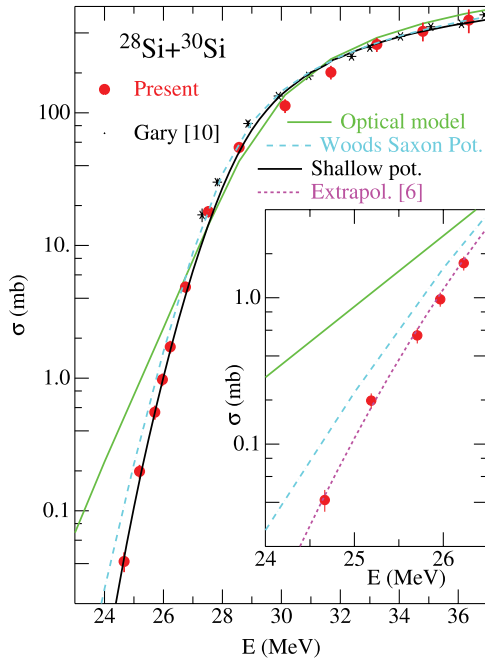


FIG. 1. (Color online) Comparisons of experimental evaporation residue cross sections with various calculations for the system $^{28}\text{Si} + ^{30}\text{Si}$. Green solid: optical model, black: CC with shallow potential. Light-blue dash-dotted: CC with Woods-Saxon potential. Magenta dotted: an extrapolation corresponding to the curve: $L(E) = A_0 + B_0/E^{1.5}$ in Fig. 3(a).

background from scattered beam particles and other reaction particles increased strongly (to $\sim 30\%$) and prevented us from extending the excitation function to lower energies.

The experimental cross sections (red circles) are presented in Fig. 1, as a function of center-of-mass energy E . While the normalization of the data in the most interesting energy region below 31 MeV is straightforward, one has to consider that for four data points at higher energies ($E = 31.7\text{--}36.4$ MeV), the elastic scattering at the monitor angles of 45° is not pure Rutherford in character. In this energy range we have, therefore, used optical model calculations with the potential parameters from Ref. [13] ($V = 100$ MeV, $W = 10$ MeV, $r_0 = 1.20$ fm, $r_{0i} = 1.28$ fm, $a_0 = 0.46$ fm and $a_i = 0.39$ fm), obtained from a fit to the elastic scattering of $^{28}\text{Si} + ^{30}\text{Si}$ at energies of 33.6 and 36.2 MeV. The fusion cross sections obtained with this potential are shown by the green curve in Fig. 1. At the higher energies, the calculations are in good agreement with both the present and previous [9] cross sections. At the lowest energies, however, the optical model calculations overpredict the fusion cross sections by a factor of more than 10. A similar behavior has been observed for many lighter systems where a standard average potential ($V = 50$ MeV, $W = 10$ MeV, $r_0 = r_{0i} = 1.28$ fm and $a_0 = a_i = 0.4$ fm, [14]) gives good agreement at the higher energies, but overpredicts the fusion cross sections at very low energies [6,15]. It should be noted that the calculated fusion cross sections obtained by these two sets of potential parameters are nearly identical over the whole energy range under investigation (23–37 MeV).

TABLE I. States and corresponding parameters used in the CC calculations for nuclei ^{28}Si and ^{30}Si (from Refs. [18,19]).

Nucleus	λ^π	E_x (MeV)	$B(E\lambda)$ (W.U.)	β_λ^C	β_λ^N
^{28}Si	2^+	1.78	13.2	-0.41	-0.41
	$2\text{PH}(2)^+$	4.69	8.8	-0.24	-0.24
	3^-	6.88	13.9	0.42	0.42
^{30}Si	2^+	2.24	7.4	0.31	0.31
	$2\text{PH}(2)^+$	4.31	5.2	0.18	0.18
	3^-	5.49	6.1 [19]	0.27	0.27

Standard coupled-channels calculations (CC) with a Woods-Saxon (WS) nuclear potential from Akyüz and Winther [16] are shown by the light-blue dash-dotted curve. The excited states of ^{28}Si and ^{30}Si included in the CC calculations are listed in Table I along with their excitation energies, and the values of the reduced electric quadrupole transition probability, $B(E\lambda)$ and the deformation parameter, β . While they give in general a better agreement, they still overpredict the cross sections at the lowest energies (see insert in Fig. 1).

In Ref. [17] a model was suggested to explain the fusion hindrance by including the saturation property of nuclear matter. This model introduces a repulsive core, resulting in a shallow potential, and has reproduced the hindrance behavior observed in many systems with negative Q -values, such as $^{64}\text{Ni} + ^{64}\text{Ni}$ [17]. The same recipe is used here. The potential used is the M3Y potential added to a repulsive core. The calculations of the repulsive core are based on a nuclear incompressibility of $K = 234$ MeV and a diffuseness a_{rep} of the hard core density varying within the 0.410–0.425 fm range. These potentials are compared in Fig. 2 with the standard Woods-Saxon (WS) potential. It is evident that the M3Y+repulsive potentials lead to a shallower pocket as compared to the WS potential. The best fit to the present data is achieved with $a_{\text{rep}} = 0.415$ fm. The resulting cross sections are given in Fig. 1 by the black curve. This CC calculation with a shallow potential reproduces the experimental data much better. The magenta curve is an

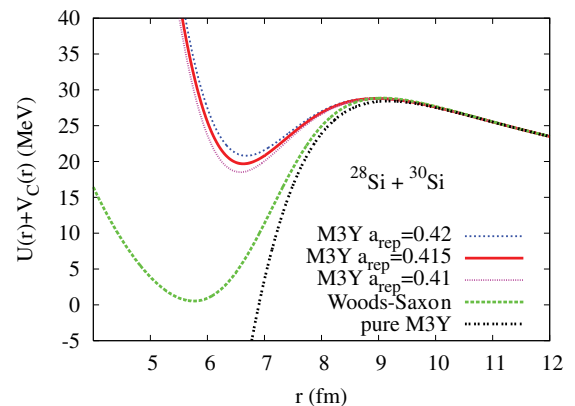


FIG. 2. (Color online) Comparison of potentials used in the CC calculations. For Ref. [17], different diffusenesses a_{rep} of the hard core density are used ($a_{\text{rep}} = 0.42, 0.415, 0.41$ fm, respectively). The black double-dotted curve is the pure M3Y potential.

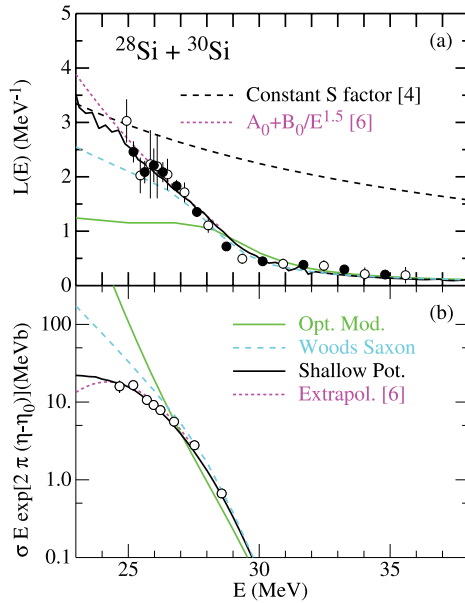


FIG. 3. (Color online) (a) The logarithmic derivative $L(E) = d(\ln \sigma E)/dE$ plotted as a function of the center-of-mass energy E . The solid circles were derived from the data by least-squares fits to three consecutive data points while the open circles were obtained with the two-points method. The magenta dotted curve is a fit to the low energy part of the data with a formula $L(E) = A_0 + B_0/E^{1.5}$. (b) The S factor versus E plot. The magenta dotted curve is an extrapolated one. See text for details.

extrapolation obtained with the recipe developed in Ref. [6] (see the insert), which will be discussed in the next paragraph.

The conversions of the fusion cross sections to either logarithmic derivatives, $L(E) = d \ln(\sigma E)/dE$ or an S factor are given in Fig. 3. The solid circles for the $L(E)$ values were derived from the data by least-squares fits to three consecutive data points, while the open circles were obtained with the two-points method. The dashed curve in Fig. 3(a) corresponds to the constant S factor function $L_{cs}(E) = \frac{\pi\eta}{E}$, where η is the Sommerfeld parameter [4]. The dotted magenta curve in Fig. 3(a) corresponds to a fit to the low energy part of the experimental data with the formula suggested in Ref. [6]:

$$L(E) = A_0 + B_0/E^{1.5} \text{ MeV}^{-1}. \quad (1)$$

The dotted magenta curve in Fig. 3(b) is in turn the extrapolation corresponding to the magenta curve in Fig. 3(a), which is also developed in Ref. [6]. In Fig. 3, the calculations with the optical model, standard coupled-channels and coupled-channels with a shallow potential are shown with the same colors and definitions as in Fig. 1. Figure 3(b) clearly demonstrates that the optical model and the standard CC calculations overpredict the data by a large amount, while the CC calculations with a shallow potential represent the data rather well.

From the definition of the constant S factor function, the intersection point (L_s and E_s) of the lines $L(E)$ and $L_{cs}(E)$ corresponds to the location of the maximum of the S factor. From previous studies, we concluded that the observation of a maximum signals the onset of sub-barrier fusion hindrance. A maximum of the S factor cannot be

reproduced either by standard coupled-channels calculations for negative Q -value systems, or by optical model calculations for positive Q -value systems. Since the lowest energy point in the measured excitation function is at $E = 24.67$ MeV, the intersection between $L(E)$ and $L_{cs}(E)$ can be inferred only from a single point derived with the two-points method in the present experiment. As a result, no maximum in the S factor (Fig. 3(b)) has been observed with certainty. Depending on the extrapolation, this maximum might occur at an energy below 24.7 MeV. There is a systematic study about the radius-of-curvature, ρ , of the S factor maximum in Ref. [5]. From this study, the maximum of the S factor in the system $^{28}\text{Si} + ^{30}\text{Si}$ could be a broad one, since one obtains a large predicted ρ value from Eq. (8) of Ref. [5].

While no conclusion about a maximum for the S factor can be drawn from the data, it is obvious from Figs. 1 and 3, however, that optical model calculations, which have been extensively used in the past in extrapolations of fusion cross sections to lower energies especially for systems of astrophysical interest, do not result in a satisfactory description of the data. They predict a continuous increase of the S factor toward lower energies, which is at variance with the data by more than an order of magnitude. On the other hand, the calculations with a shallow potential model do reproduce the present data. Thus, it appears that the present experimental results support the conclusion given in the previous systematical study [5,6] that the fusion hindrance occurs also in systems with positive Q -values.

From the definition of $L(E) = d \ln(\sigma E)/dE$ it is clear that $L(E) \rightarrow \infty$ for $E \rightarrow 0$ in systems with $Q > 0$, whereas for $Q < 0$, $L(E) \rightarrow \infty$ for $E \rightarrow -Q$, because the cross section must vanish at the energy corresponding to the ground state of the fusing system. This implies that the slope of the logarithmic dependence of σE as a function of E becomes steeper with a decrease in energy, as demonstrated experimentally in Ref. [5] from an analysis of many systems.

For a negative Q -value system, $S(E) \rightarrow 0$ when $E \rightarrow -Q$. This leads to the conclusion that for negative Q -value systems, a maximum in the S factor must occur at low energies, which cannot be reproduced by the standard coupled channels calculations. For a positive Q -value system, however, there is no restriction on $S(E)$ when $E \rightarrow 0$. There are many indications, however, that the general tendency of the measured S factor is to exhibit a decrease at the lowest energies, which can also not be reproduced by optical model calculations [6].

Recently, coupled channels calculations have been performed for lighter heavy-ion systems, such as $^{16}\text{O} + ^{16}\text{O}$ [20]. With the same parameters obtained in the present calculations for the system $^{28}\text{Si} + ^{30}\text{Si}$ ($K = 234$ MeV and $a_{\text{res}} = 0.415$ fm), the shallow potential model can also reproduce the low energy data of $^{16}\text{O} + ^{16}\text{O}$, and even the extrapolations obtained with the fusion hindrance recipe [6]. Since this model, which was developed to explain the hindrance for negative Q -value systems, can also reproduce the low energy data for the positive Q -value systems $^{28}\text{Si} + ^{30}\text{Si}$ and $^{16}\text{O} + ^{16}\text{O}$, it appears likely that the saturation property of nuclear matter influences the fusion of these positive Q -value systems as well, and results in the hindrance of the fusion process.

In conclusion, the first measurement studying heavy-ion fusion hindrance in a light system with a positive Q -value, $^{28}\text{Si} + ^{30}\text{Si}$, has been reported. While the excitation function could not be measured down to sufficiently low cross sections to exhibit a clear maximum in the S factor, and thus indicate firmly the occurrence of fusion hindrance in systems with positive Q -values, strong deviations from the optical model predictions and the standard CC calculations have been observed. The present results appear to support that fusion hindrance occurs for positive Q -value systems. Since optical model calculations (and other potential penetration

models, like the ones used in Ref. [21,22]) are frequently used to extrapolate experimental cross sections toward lower, astrophysically interesting energies, these results will also influence the field of nuclear astrophysics, e.g., supernovae and pycnonuclear burnings, where heavy-ion fusion plays an important role.

This work was supported by the U.S. Department of Energy, Office of Nuclear Physics, under Contract No. DE-AC02-06CH11357.

-
- [1] C. L. Jiang *et al.*, Phys. Rev. Lett. **89**, 052701 (2002); **93**, 012701 (2004); Phys. Rev. C **71**, 044613 (2005); Phys. Lett. **B640**, 18 (2006).
- [2] M. Dasgupta *et al.*, Phys. Rev. Lett. **99**, 192701 (2007).
- [3] M. Trotta *et al.*, Nucl. Phys. **A787**, 134c (2007).
- [4] C. L. Jiang, H. Esbensen, B. B. Back, R. V. F. Janssens, and K. E. Rehm, Phys. Rev. C **69**, 014604 (2004).
- [5] C. L. Jiang, B. B. Back, H. Esbensen, R. V. F. Janssens, and K. E. Rehm, Phys. Rev. C **73**, 014613 (2006).
- [6] C. L. Jiang, K. E. Rehm, B. B. Back, and R. V. F. Janssens, Phys. Rev. C **75**, 015803 (2007).
- [7] C. L. Jiang, B. B. Back, R. V. F. Janssens, and K. E. Rehm, Phys. Rev. C **75**, 057604 (2007).
- [8] L. R. Gasques *et al.*, Phys. Rev. C **76**, 035802 (2007).
- [9] S. Gary and C. Volant, Phys. Rev. C **25**, 1877 (1982).
- [10] C. N. Davids and J. D. Larson, Nucl. Instrum. Methods Phys. Res. B **40**, 1224 (1989); C. N. Davids *et al.*, *ibid.* **70**, 358 (1992).
- [11] C. L. Jiang *et al.*, Nucl. Instrum. Methods A **554**, 500 (2005).
- [12] A. Gavron, Phys. Rev. C **21**, 230 (1980).
- [13] K. D. Hildenbrand *et al.*, Nucl. Phys. **A234**, 167 (1974).
- [14] G. J. Michaud and E. W. Vogt, Phys. Rev. C **5**, 350 (1972); G. J. Michaud, *ibid.* **8**, 525 (1973).
- [15] R. G. Stokstad *et al.*, Phys. Rev. Lett. **37**, 888 (1976).
- [16] Ö. Akyüz and A. Winther, in *Proceedings of the Enrico Fermi School of Physics, 1979, Course on Nuclear Structure and Heavy-Ion Reactions*, edited by R. A. Broglia, C. H. Dasso and R. Ricci (North Holland, Amsterdam, 1981).
- [17] S. Mişicu and H. Esbensen, Phys. Rev. Lett. **96**, 112701 (2006).
- [18] Evaluated Nuclear Structure Data Files, National Nuclear Data Center, Brookhaven National Laboratory: <http://www.nndc.bnl.gov/>.
- [19] R. H. Spear, At. Data Nucl. Data Tables **42**, 55 (1999).
- [20] H. Esbensen, Phys. Rev. C **77**, 054608 (2008).
- [21] L. R. Gasques *et al.*, Phys. Rev. C **72**, 025806 (2005).
- [22] C. J. Horowitz and H. Dussan, Phys. Rev. C **77**, 045807 (2008).